Applied Catalysis B: Environmental 341 (2024) 123345

Contents lists available at ScienceDirect

Applied Catalysis B: Environmental

journal homepage: www.elsevier.com/locate/apcatb

How flue gas impurities affect the electrochemical reduction of CO_2 to CO and formate

Sam Van Daele [a], Lieven Hintjens [a], Saskia Hoekx [a,b], Barbara Bohlen [a], Sander Neukermans [a], Nick Daems [a], Jonas Hereijgers [a], Tom Breugelmans [a,*]

[a] Research Group Applied Electrochemistry & Catalysis (ELCAT), University of Antwerp, Universiteitsplein 1, Wilrijk 2610, Antwerp, Belgium
[b] Electron Microscopy for Materials Science (EMAT), University of Antwerp, Groenenborgerlaan 171, Wilrijk 2610, Antwerp, Belgium

ARTICLE INFO

Keywords:
CO2 reduction
Impurities
Electrochemistry
Formate
CO

ABSTRACT

The electrochemical CO_2 reduction offers a promising solution to convert waste CO_2 into valuable products like CO and formate. However, CO_2 capture and purification remains an energy intensive process and therefore the direct usage of industrially available waste CO_2 streams containing SO_2, NO and O_2 impurities becomes more interesting. This work demonstrates an efficient (Faradaic efficiency > 90 %) and stable performance over 20 h with 200 ppm SO_2 or NO in the feed gas stream. However, the addition of 1 % O_2 to the CO_2 feed causes a significant drop in Faradaic efficiency to C-products due to the competitive oxygen reduction reaction. A potential mitigation strategy is to operate at higher total current density to firstly reduce most O_2 and achieve sufficient product output from CO_2 reduction. These results aid in understanding the impact of flue gas impurities during CO_2 electrolysis which is crucial for potentially bypassing the CO_2 purification step.

1. Introduction

As CO_2 emissions continue to increase globally, finding sustainable ways to capture and utilize CO_2 has become a pressing issue [1]. The electrochemical CO_2 reduction reaction (CO_2RR) has emerged as a promising and sustainable approach to convert CO_2 into value-added fuels and chemicals like carbon monoxide, formic acid, ethylene, ethanol, acetic acid and n-propanol [2]. Especially the production of carbon monoxide and formic acid are of particular interest because they only require a two electron transfer and benefit from great revenue per mole of electron transfer [3]. Different pilot scale plants producing formic acid or CO have been installed in the last years and the focus on industrial relevant conditions in literature is becoming the norm [4,5]. However, almost all research in this field has been conducted using pure CO_2 which would come from captured and purified CO_2 point sources. These processes are considered as energy intensive [6]. For example, the energy demand for carbon capture with monoethanolamine is ~ 3.7 GJ/ton CO_2 [7]. The estimated cost of CO_2 capture from a biomass-based combustion power plant are in the range of \$150–400/tCO_2. Additionally, the associated purification costs are reported to be \$70–275/tCO_2 [8]. Direct utilization of CO_2 from flue gas point sources can be immensely interesting from an economical perspective as it allows to bypass the capture and purification steps. Untreated flue gas streams contain different gaseous impurities (Table 1) that can affect the performance of CO_2 electrolyzers. Thus, understanding the influence of impurities during CO_2 electrolysis is crucial for the practical application of this technology.

The concentration of each impurity is highly dependent on the point source and therefore also the type of industry. Table 1 summarizes the typical concentration of flue gases. On average, CO_2 is mostly present in diluted form with > 70 % N_2. The steel and cement industry have the highest concentrations of CO_2 in their flue gas stream, i.e., > 25 %. The impact of N_2-dilution was studied in our previous work, which indicated that formate is preferred over CO as target product in diluted CO_2 as it maintained a higher efficiency even at low CO_2 contents (i.e., down to 10 % CO_2). It was discovered that the main reason for this behavior, was the difference in hydroxide production and subsequent CO_2 neutralization as (bi)carbonate. Whereas CO is accompanied by the formation of two hydroxide ions, only one hydroxide ion is generated with formate production, hence less CO_2 neutralization occurs when formate is targeted and more CO_2 remains available for reaction [9].

Secondly, while the O_2 impurity has been investigated in a few reports, the focus was solely on the use of Cu catalysts for producing C_{2+}-products and was mostly performed in an H-type cell at low current

* Corresponding author.
E-mail address: Tom.Breugelmans@uantwerpen.be (T. Breugelmans).

https://doi.org/10.1016/j.apcatb.2023.123345
Received 7 June 2023; Received in revised form 7 September 2023; Accepted 25 September 2023
Available online 1 October 2023

densities [15–18]. Furthermore, only one or two fixed concentrations of oxygen were typically investigated. The above clearly indicates that, especially for CO- or formate producing catalysts, the impact of different O_2 concentrations on the CO_2RR remains largely unexplored, even more so at industrially relevant conditions in a continuous flow cell. This work is thus to the best of our knowledge the first study thoroughly investigating the impact of O_2 on the CO_2RR to formate and CO.

The impact of NO_x (of wich NO is the most abundant) has been studied on Cu, Ag and Sn catalysts by introducing 8300 ppm NO in a CO_2 stream at 100 mA/cm^2 for 30 min [19]. For Ag and Sn catalysts, the loss of Faradaic efficiency (FE) was found to be ~ 35 % due to NO reduction reactions. Similarly, the introduction of 10 000 ppm SO_x also caused a 25–40 % FE loss when targeting CO or formate [20]. In both cases, the original FEs are restored again when a pure CO_2 stream is re-introduced in the reactor [19,20]. Even though these articles contain a very thorough analysis of these effects, the question remains whether flue gas-like concentrations of SO_x and NO (~ 200 ppm, Table 1) affect the catalyst stability on the long term and will be evaluated here.

This work focuses on the effects of SO_2 and NO impurities during 20 h CO_2 electrolysis in a flow cell and demonstrates that ~ 200 ppm of these compounds are compatible with CO_2RR. Furthermore, we investigate the influence of O_2 during CO_2RR and suggest a strategy to boost partial current densities to the target products CO (Ag catalyst) and formate (Bi_2O_3 catalyst). Knowledge about the interference between gaseous impurities and CO_2RR is critical for the practical application of this technology, and could allow industrial plants to omit or significantly decrease the number of necessary purification steps to enhance economical viability.

2. Materials and methods

2.1. Chemicals and products

Potassium bicarbonate (> 99.5 %) and potassium hydroxide (> 85 %) for electrolyte preparation were purchased from Chem-lab. Ultrapure water (Milli-Q, Millipore) with a resistivity of 18.2 MΩ · cm was used to obtain the desired concentration of reagents (0.5 M $KHCO_3$ and 1 M KOH). Commercial Bi_2O_3 nanoparticles (99.8 %, 90–210 nm, batch MKCM4378) and Ag nanoparticles (99.5 %, < 100 nm, batch MKCP1973) were purchased from Sigma-Aldrich. Iso-propanol for catalyst ink preparation was purchased from Chem-lab. A perfluorinated nafion dispersion (D520, 5 % w/w in water and 1-propanol) was purchased from Thermo Fisher Scientific and used as binder in the catalyst inks. Perchloric acid (70 %) was purchased from Chem-lab and diluted to a 1.2 M solution to be used during sample preparation for HPLC analysis. Sulfuric acid (98 + % HPLC grade) was purchased from Chem-lab and used to prepare the 10 mM H_2SO_4 mobile phase for HPLC analysis. Nafion 117 cation exchange membrane were purchased from Ion Power. Hydrogen peroxide (30 %) was purchased from VWR and diluted to 3 % for use during membrane activation.

2.2. Gases

Argon (99.999 %) for spray coating, helium (99.999 %) for gas chromatography analysis and CO_2 (99.998 %) for experiments without impurities were purchased from Air Liquide. For the SO_2 and NO experiments, a mixture of 213 ppm SO_2 in CO_2 and 198 ppm NO in CO_2 was purchased from Nippon gases. A mixture of 19.96 % O_2 in CO_2 was purchased from Nippon gases for the experiments with an oxygen impurity.

2.3. Gas diffusion electrodes

Catalyst inks were made by mixing 72 mg of either commercial Bi_2O_3 nanoparticles or commercial Ag nanoparticles with 200 mg (5 w%) nafion dispersion, iso-propanol (99.8 %, Chem-lab) and ultrapure water. The volumetric ratio water: iso-propanol was 1:2 and 1:4 for Ag and Bi_2O_3 respectively. After preparation, the ink was sonicated (NexT-gen Lab120) for at least 30 min with a 6 mm titanium probe (34 kHz, 84 µm amplitude). The substrate, a Sigracet GDL 39BB (Ion Power), was fixed on a hot plate at 80°C to improve drying. The ink was spray coated with a Fengda BD-183 airbrush equiped with 0.3 mm nozzle using argon as carrier gas. The GDE was weighed before and after to ensure a 2 mg/cm^2 catalyst loading on all samples. The geometrical active surface area is 10 cm^2. Light microscopic and scanning electron microscopic images of the as-perepared GDEs can be found in the supplementary information (SI) Fig. S.1 as well as TEM (Figs. S.2-S.3) and XRD (Figs. S.4-S.5) measurements on the catalytic nanoparticles.

2.4. Reactor

A commercial reactor (ElectroCell Micro Flow Cell) was modified to ensure compatibility with a GDE, membrane and insertion of a Ag/AgCl reference electrode (Innovative instruments) such as reported in previous work [21]. Fig. 1 shows this electrochemical reactor with all labeled parts. The PMMA flow plates and gaskets were fabricated with a CNC mill (Euromod MP45). A pretreated Nafion 117 cation exchange membranes separates the catholyte and anolyte compartment. The pretreatment to increase its ionic conductivity and to clear the membrane from organic contaminants consists of subsequently boiling the membrane in 3% H_2O_2 (1 h), distilled water (1 h), 1 M H_2SO_4 (1 h) and distilled water (1 h) whereafter the membranes are stored at 4°C [22]. At the cathode side, 0.5 M $KHCO_3$ is supplied to the cell at 5 mL/min and at the anode, 5 mL/min of 1 M KOH is supplied to facilitate the oxygen evolution reaction. Both electrolytes are pumped through the cell with peristaltic pumps in single pass mode to ensure reliable and stable conditions during measurements. For the 20 h experiments with a SO_2 or NO

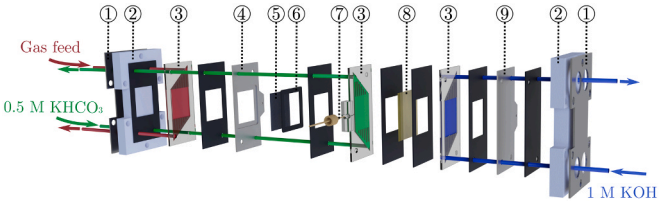

Fig. 1. Exploded view of the electrochemical reactor that was used in this study. 1) metal backplate, 2) PTFE backplate 3) PMMA gas- and liquid flow plates, 4) Titanium cathode frame, 5) gas diffusion electrode (GDE), 6) Viton gasket for GDE, 7) Ag/AgCl reference electrode, 8) Nafion 117 cation exchange membrane, 9) Platinized titanium electrode (anode). All parts are separated by rubber gaskets.

Table 1
Typical flue gas compositions.

Source	CO_2 (%)	N_2 (%)	O_2 (%)	H_2O (%)	CO (ppm)	SO_x (ppm)	NO_x (ppm)	Comments
Rajinder *et al.* [10]	13–14	70–72	3–4	6–20	–	200	200	< 10 ppm HCl/HF, 50–180°C.
Xuezhong *et al.* [11]	13.74	72.88	3.65	9.73	–	–	–	1.016 bar, 50°C.
Zhongde *et al.* [12]	11.5–14	72–76	12.5–14.5	–	160–200	0–1	135–150	0–1 ppm HCl/HF, dry flue gas reported.
Fabrizio *et al.* [13]	9–12	75–76	4–8	8–10	400–1000	150–420	100–200	15–50 ppm NH_3.
Xiaochun *et al.* [14]	7.4–7.7	73–74	~ 4.45	14.6	200–300	–	60–70	

impurity, a gas mixture of 213 ppm SO_2 or 198 ppm NO in CO_2 was controlled with an Analyt-MTC mass flow controller (50 mL/min) and fed to the reactor as illustrated in Fig. 1. For the experiments with an oxygen impurity, different feed gas compositions were obtained by mixing a 19.96% O_2 in CO_2 with pure CO_2 with a T-connection and two mass flow controllers up to a total flow rate of 100 mL/min. Chronopotentiometry experiments were conducted with an Autolab PGSTAT302N potentiostat (Metrohm) and a 10 A booster (Metrohm).

2.5. Product analysis

Liquid catholyte samples were acidified with 1.2 M $HClO_4$ in a 1:1 volumetric ratio, vortexed and filtered prior to analysis. An HPLC (Alliance 2695) equiped with a Shodex RSpak KC811 column and a PDA detector (210 nm, Waters) was used for the detection of $HCOO^-$. The acidified and filtered (0.2 µm) sample was injected in the column to quantify the amount of $HCOO^-$ produced during reactor operation.

The gas outlet of the reactor is directly connected to a gas chromatopgraph (Shimadzu) with a Restek Shincarbon ST column (1 mm internal diameter, 2 m length, mesh 100/120) that uses helium as carrier gas. Product analysis starts at 40˚C for 3 min, then temperature increases linearly at 40 ˚C/min up to 250 ˚C. The thermal conductivity detector remains at 280˚C. A Restek ProFlow 6000 flowmeter was used to measure the outgoing gas flow rate for accurate product quantification.

2.6. Characterization

Scanning electron microscopy (SEM) and energy dispersive X-ray spectroscopy (EDS) were performed on the GDE samples with a Thermo Fischer Quanta FEI 250 microscope operated at an accelerating voltage of 20 kV. High-angle annular dark field scanning transmission electron microscopy (HAADF-STEM) was performed using a Thermo Fischer Tecnai Osiris microscope operated at 200 kV. EDS maps were acquired to determine the composition of materials using a Super-X detector on the Tecnai Osiris microscope at a beam current of 50 pA. X-ray powder diffraction (XRD) measurements were performed using a Philips X'pert diffractometer with monochromated Cu-K_α ($\lambda = 1.5418$ Å) radiation.

3. Results and discussion

3.1. Long term stability with SO_2 and NO

The short-term effect of introducing great amounts of SO_2 (10 000 ppm) and NO (8300 ppm) was studied elsewhere[19,20] and results in a ± 20 % loss in FE at 100 mA/cm^2. However, most flue gases contain only around 200 ppm of these gaseous impurities [10,12,13]. To asses the impact of SO_2 and NO on the electrochemical reduction of CO_2 in a continuous flow cell, stability measurements of 20 h at 100 mA/cm^2 were carried out. Fig. 2 A and B illustrate the results with a feed stream of 198 ppm SO_2 in CO_2 with a Bi_2O_3-coated or Ag-coated GDE, respectively. The FE of Bi_2O_3-coated GDEs towards target product $HCOO^-$ remains high with on average 93.83 ± 1.35 % (average ± standard deviation) during the run without any significant loss in the total FE ($FE_{CO} + FE_{HCOO^-} + FE_{H_2}$), which was 99.04 ± 1.28 %. This observation holds as well for the Ag-coated GDE where on average 91.17 ± 1.29 % FE towards CO was observed. The electrolyzer stability and product

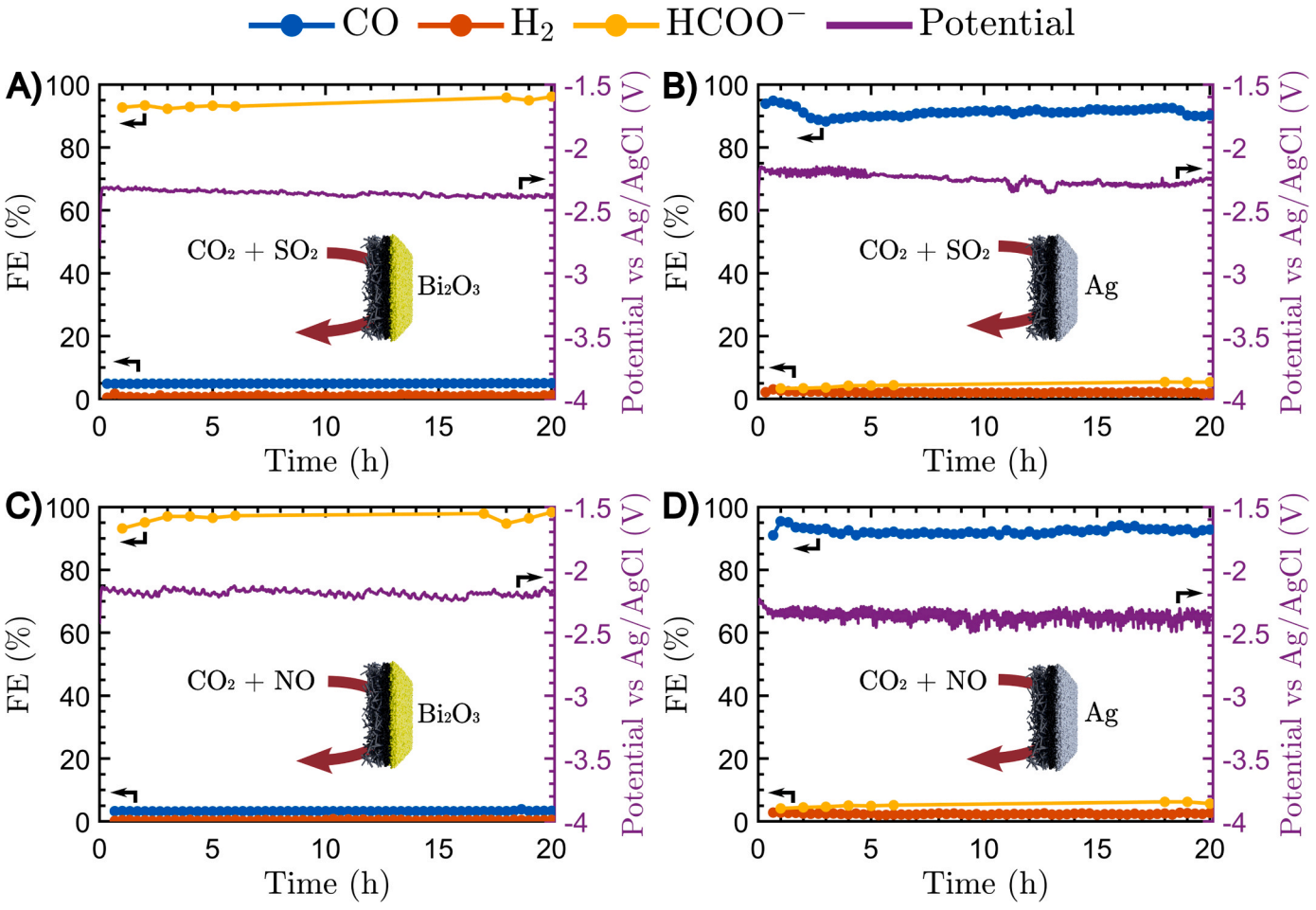

Fig. 2. Stability experiments with flue gas stream impurities. (A) 198 ppm SO_2 in CO_2 with a Bi_2O_3 catalyst. (B) 198 ppm SO_2 in CO_2 with a Ag catalyst. (C) 213 ppm NO in CO_2 with a Bi_2O_3 catalyst. (D) 213 ppm NO in CO_2 with a Ag catalyst. Experiments were conducted at 100 mA/cm^2 for 20 h at ambient conditions.

selectivity when 213 ppm NO in CO_2 was fed to the reactor is presented in a similar manner in Fig. 2 C and D. High Faradaic efficiencies to the target products $HCOO^-$ (95.06 ± 2.22 %) and CO (92.35 ± 0.92 %) were achieved for the two catalysts while observing total FE values of 99.66 ± 2.34 % and 100.26 ± 1.00 % respectively. Considering that similar efficiencies were achieved when pure CO_2 was used (SI Figures S.6 and S.7), it is clear that ~ 200 ppm SO_2 or NO in CO_2 have a negligible impact on product selectivity for 20 h. However, to confirm that these impurities did not affect the morphology or elemental composition of the catalyst layer, SEM (SI Figs. S.8, S.9) and EDS (SI Figs. S.10, S.11) measurements were carried out before and after electrolysis with pure CO_2, 198 ppm SO_2 and 213 ppm NO. Initial SEM-EDS results showed a random distribution of sulfur atoms that contained little information about the state of the particles themselves. Therefore HAADF-STEM-EDS (SI Fig. S.12, S.13) was carried out for both Bi_2O_3 and Ag coated GDEs. Fig. 3 shows the elemental mapping of sulfur before (A) and after (B) reaction with 198 ppm SO_2 on a Bi_2O_3 coated and Ag coated GDE before (C) and after (D) reaction. According to the analysis, the signal map for sulfur was found to be evenly distributed, and it is therefore highly likely that this signal arises from the Nafion binder used in the catalyst ink preparation. Alternatively, the signal could also be influenced by other atoms, such as carbon, oxygen, and nitrogen that have X-ray energies similar to that of sulfur, potentially leading to interference [23]. Our results did not show a clear and dense sulfur signal at the edges of the particles as seen in experiments with 10, 000 ppm SO_2 where small amounts of metal sulfides were observed [20]. In fact, there was never more than 0.3 wt% sulfur detected (after 20 h electrolysis) such that the effect of impurity incorporation for ~ 200 ppm SO_2 seems negligible. Further HAADF-STEM-EDS measurements (SI Figs. S.14, S.15) also suggest no impurity incorporation from NO into the catalyst layer, which aligns with the observation from Ko *et al* [19]. Besides this, a color change from yellow to dark blue/black of the Bi_2O_3 catalyst layer was examined after every experiment where a reducing potential was applied to the GDE, which was attributed to the in-situ reduction of Bi_2O_3 to Bi. Additionally, the SEM-analysis of this Bi_2O_3 catalyst layer before (Fig. 3 E) and after (Fig. 3 F) electrolysis reveals that the particles underwent a serious morphology change that goes beyond commonly reported agglomeration of nanoparticles or other degradation mechanisms [24]. In contrast to the negative effects associated with degradation mechanisms, this morphology change to a flower-like structure is reported to be beneficial for CO_2 reduction [25]. As a matter of fact, Liu *et al.* introduced the synthesis of these structures through reactions with Bi, O_2 and CO_2 to form flower-like $Bi_2O_2CO_3$ sites with excellent CO_2 adsorption and conversion properties due to the great catalytic surface area [25]. The structural change observed in the experiments cannot be ascribed to the introduction of SO_2 or NO into CO_2 feed streams, as it also occurs in experiments with pure CO_2 and is a result of applying current to the catalyst. Altogether, the consequences on the performance of adding ~ 200 ppm NO or SO_2 at 100 mA/cm^2 seem minimal. To further increase the industrial viabilitiy, higher

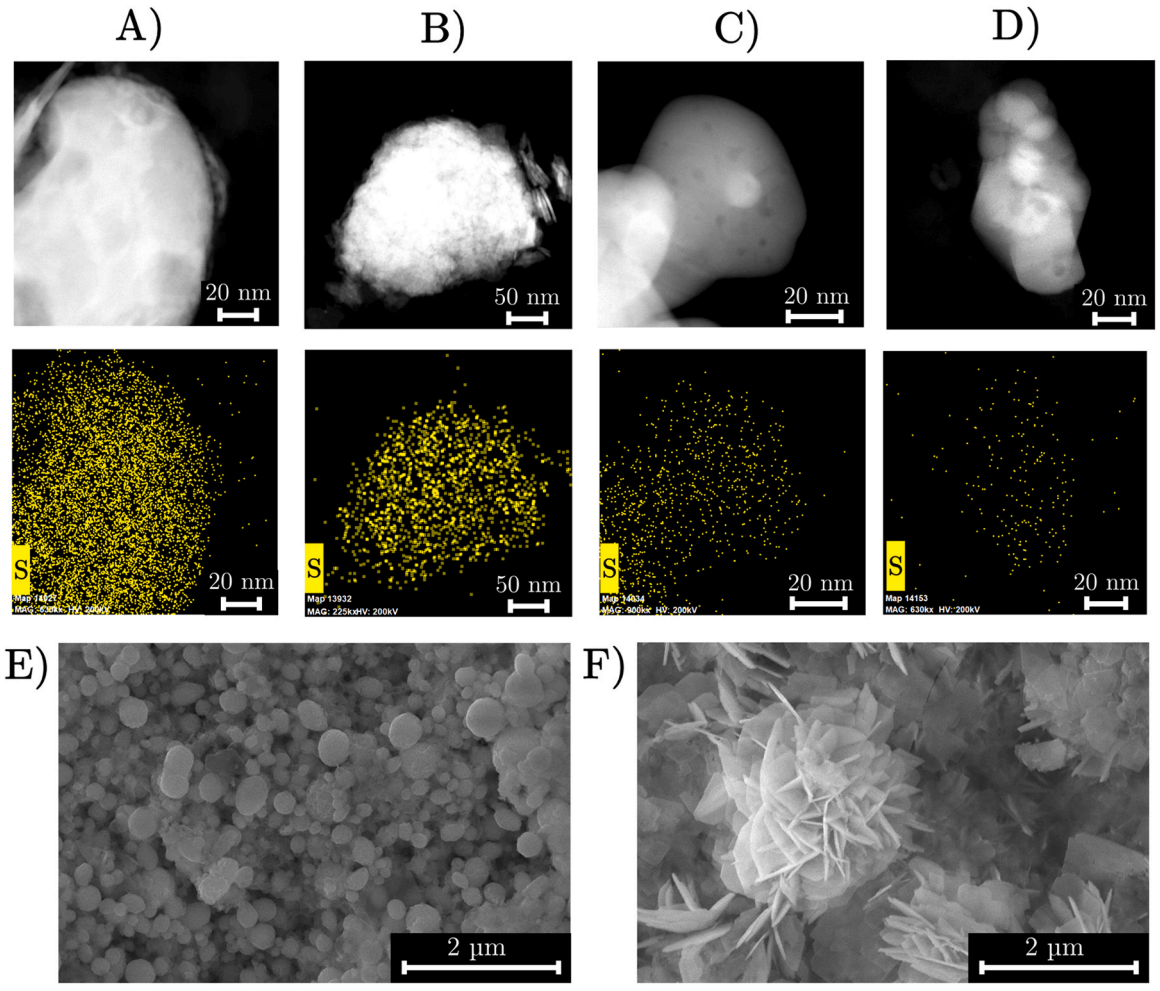

Fig. 3. HAADF-STEM images with their respective EDS map of sulfur and SEM images. (A) HAADF-STEM-EDS of Bi_2O_3 from the GDE after spray-coating. (B) HAADF-STEM-EDS of Bi_2O_3 after 20 h electrolysis with 198 ppm SO_2 in CO_2. (C) HAADF-STEM-EDS of Ag from the GDE after spray-coating. (D) HAADF-STEM-EDS of Ag after 20 h electrolysis with 198 ppm SO_2 in CO_2. (E) SEM-image of Bi_2O_3 nanoparticles on the GDE after spray-coating. (F) SEM image of Bi_2O_3 nanoparticles on the GDE after electrolysis with pure CO_2.

current densities and thus higher product outputs were also considered here. Upon increasing the current density to 200 mA/cm^2, a similar product selectivity and stability of the reactor is maintained (SI Figs S.16-S.21). Considering all of the above (high FE (> 90 %), no sulfur incorporation and stable reactor performance), it is clear that these impurity levels are compatible with CO_2 reduction. These findings suggest that the removal of ~ 200 ppm SO_2 or NO is not necessary to maintain good electrolyzer performance which raises economical viability of the technology.

3.2. Impact of different oxygen concentrations in the feed gas stream

Another important component that is present in one order of magnitude higher than SO_2 or NO in flue gases, is oxygen. It is abundant in the air and obviously necessary in any combustion process to generate CO_2. To assess the influence of oxygen during CO_2 electrolysis, chronopotentiometry measurements were started at 100 mA/cm^2 with pure CO_2 for 30 min, afterwards the oxygen content of the gas feed was increased by 1% for approximately 1 h until three gas samples from the outflow could have been analyzed by gas chromatography. This process was repeated up to 5 % O_2 while restoring a pure CO_2 feed in between different O_2 contents to verify whether or not the O_2 impurity would permanently affect the catalyst layer and consequently, the product selectivity of the CO_2RR or if performance can be restored upon its removal from the reactor. Fig. 4 A shows the results with a Bi_2O_3 catalyst. The effects of oxygen in the feed stream are already visible for O_2 concentrations as low as 1 % where 23 % of the FE is lost and clearly indicates that oxygen heavily affects the CO_2 reduction product output. After re-introducing a pure CO_2 gas feed to the reactor, original Faradaic efficiencies are recovered. This observation indicates that there is no impact on catalyst stability, and therefore suggests that the influence is limited to the occurrence of competitive electrochemical reaction(s) and thus O_2 instead of CO_2 reduction. The addition of O_2 is also accompanied by a change in potential to a less negative value (for example − 1.62 V at 5 % O_2) compared to pure CO_2 (−2.33 V). Similar losses in FE were obtained for the Ag catalyst (Fig. 4 B) albeit at even less negative potentials (e.g., with 5 % O_2, − 1.38 V was only needed) and this will be revisited and discussed later on. The reactor was again operated in galvanostatic mode (i.e., constant current) and the oxygen concentration was altered every 30 min for 0–5 %, 10 %, 15 % and 20 % O_2 in CO_2 and the results are presented in Fig. 4 C and D for Bi_2O_3 and Ag respectively. A proportional relationship between total FE and oxygen feed composition can be observed for the two catalysts at 0–5 % O_2. More specifically, a linear trend can be derived from the results with a slope of − 19.39 %FE/%O_2 for Bi_2O_3 and − 18.958 %FE/%O_2 for Ag (SI Fig. S.22). Fig. 4 C and D both display an increasing trend in potential (less negative) towards higher O_2 concentrations showing that the competitive reaction is clearly more favorable than CO_2RR to $HCOO^-$ or CO. At 20 % O_2, the potential with Bi_2O_3 reads − 1.35 ± 0.04 V (Fig. 4 C) compared to − 0.99 ± 0.01 V (Fig. 4 D) with Ag. The original potentials with a pure CO_2 stream are very similar, more specifically, − 2.33 ± 0.03 V for Bi_2O_3 and − 2.32 ± 0.16 V for Ag. Based on the 0.36 V difference with 20 % O_2, it can be derived that the competitive reaction is catalytic in nature. This is because the reaction appears to be facilitated more easily by Ag, thus demanding a lower overpotential to achieve the desired current density. Indeed, the oxygen reduction reaction (ORR) is a known catalytic reaction that can occur under reducing potentials and is thermodynamically more favorable than CO_2RR to CO

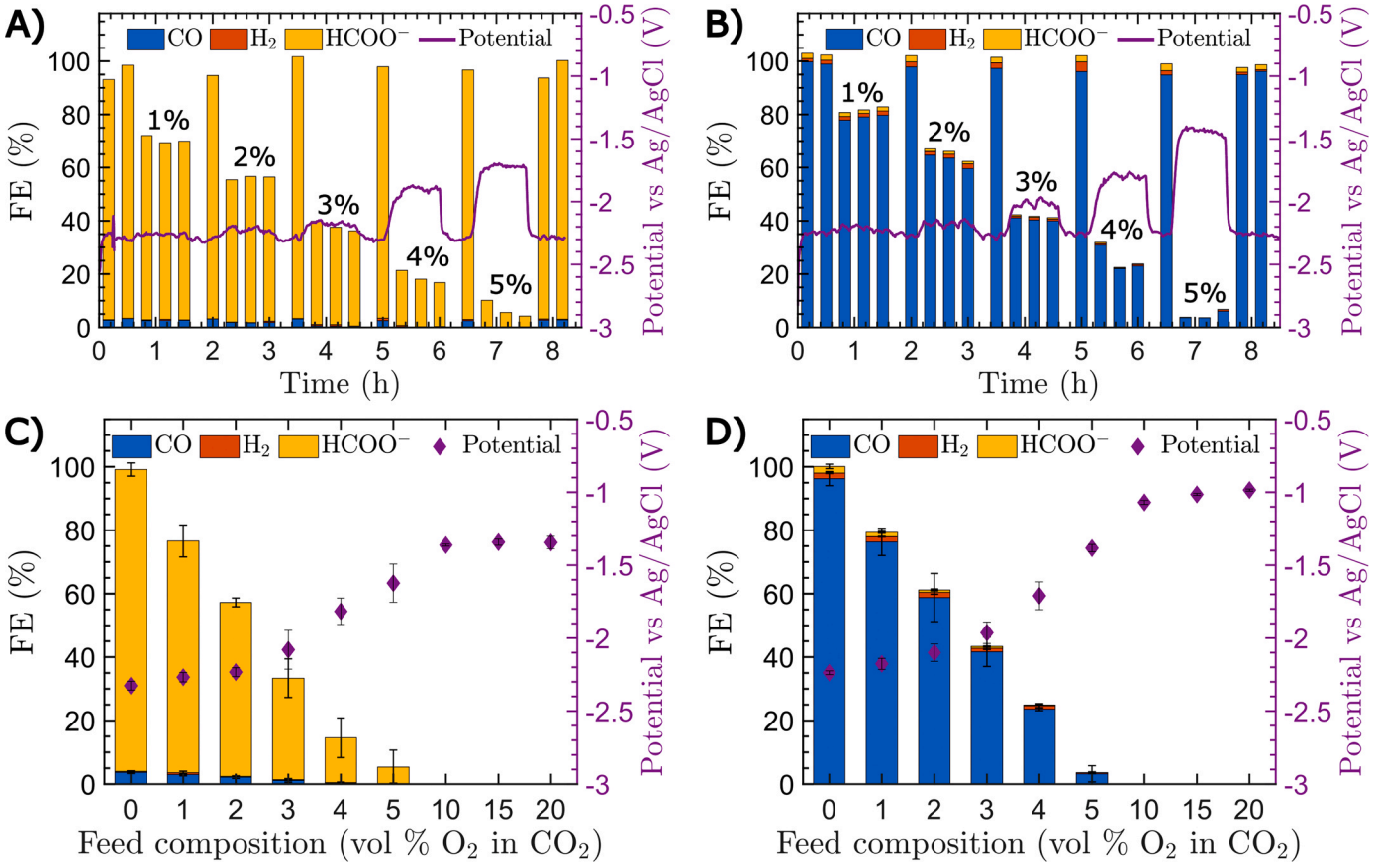

Fig. 4. Faradaic efficiency and reference electrode potential for different O_2 concentrations in the CO_2 feed gas stream. (A) Single run for 1–5 % O_2 in CO_2 with a Bi_2O_3 catalyst and intermediate checks with pure CO_2. (B) Single run for 1–5 % O_2 in CO_2 with a Ag catalyst and intermediate checks with pure CO_2. (C) Faradaic efficiency for 0–20 % O_2 in CO_2 with Bi_2O_3 catalyst. (D) Faradaic efficiency for 0–20 % O_2 in CO_2 with Ag catalyst. Experiments were performed at 100 mA/cm^2 with a total gas flow rate of 100 mL/min. Error bars represent standard deviation from three experiments.

or $HCOO^-$ [26]. Especially Ag-based catalysts are reported to be interesting for ORR in alkaline environments [27], which reflects the conditions in the vicinity of the electrode during CO_2RR due to the local OH^- generation by CO_2RR [9,28]. In alkaline environments, Equations (1) and (2) represent the four- and two-electron pathway of ORR respectively.

$$O_2 + 2H_2O + 4e^- \leftrightharpoons 4OH^- \quad (1)$$

$$O_2 + H_2O + 2e^- \leftrightharpoons HO_2^- + OH^- \quad (2)$$

The two-electron pathway may be followed by a further reduction given in Equation (3).

$$HO_2^- + H_2O + 2e^- \leftrightharpoons 3OH^- \quad (3)$$

On the other hand, the HO_2^- can undergo a disproportionation reaction towards OH^- and O_2 (Equation (4)).

$$2HO_2^- \leftrightharpoons 2OH^- + O_2 \quad (4)$$

The accurate quantification of ORR products during CO_2RR remains difficult because OH^- ions are also formed as by-products from CO_2RR and participate in more equilibrium reactions [28]. However, to validate the consumption of O_2 and consequently the appearance of ORR at the cathode, gas chromatograms of 3 % O_2 in CO_2 were compared and illustrated in Fig. 5. For both Bi_2O_3 and Ag, the oxygen peak height decreased significantly by almost 70 % when current was applied compared to the oxygen signal in the 3 % O_2 in CO_2 mixture without any current. These results confirm that the oxygen impurity is subjected to a reduction reaction whereby less electrons can participate in any CO_2RR thus lowering the overall FE of the system.

3.3. The effect of current density on the CO_2RR with oxygen

The previous results show a clear influence of oxygen contaminants in the gas feed stream during CO_2RR. An increment in oxygen concentration causes a proportional loss in total FE. This raises the hypothesis

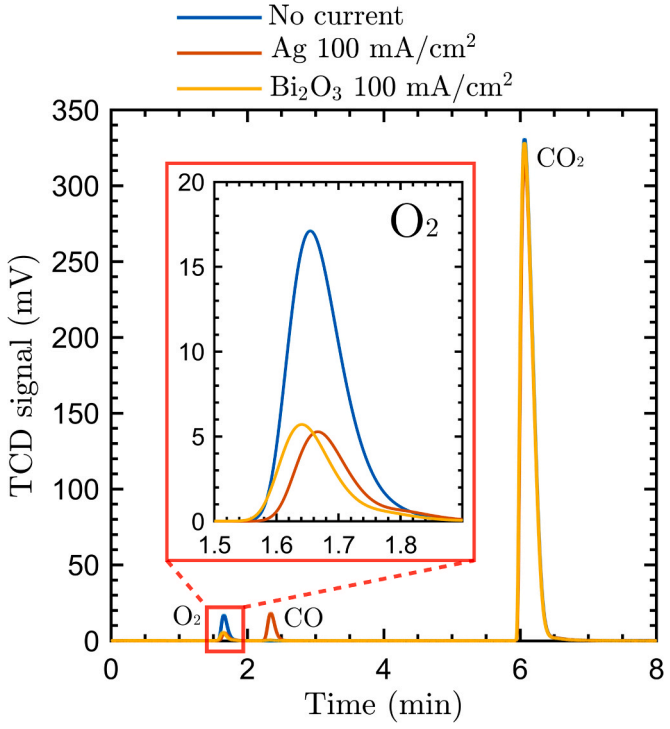

Fig. 5. Comparison of gas chromatographs from a 3 % O_2 in CO_2 gas stream that was fed to the reactor. The graph shows the detector signal without any current applied and with Ag or Bi_2O_3 coated carbon paper at 100 mA/cm^2.

that any CO_2RR can only take place after all O_2 near the electrode is reduced and oxygen becomes mass transport limited. In order to test this hypothesis and explore the impact of varying current densities on the electrolyzer, different feed gas streams containing 0, 1, 3, or 6 % O_2 in CO_2 were used in the reactor and the current density was adjusted every 20 min within a range of 25–300 mA/cm^2. Gas and liquid samples were acquired each time.

Fig. 6 A-D represents the results for the Bi_2O_3 GDE. When a pure CO_2 stream is supplied to the reactor, the catalyst remains extremely selective to $HCOO^-$ at 300 mA/cm^2 with $FE_{HCOO^-} = 93.70 \pm 1.31$ %, $FE_{CO} = 6.13 \pm 2.11$ % and $FE_{H_2} = 0.86 \pm 0.20$ %. At 25 mA/cm^2, the addition of only 1% O_2 causes a tremendous decrease of FE to target product $HCOO^-$ to merely 13.42 ± 1.92 % (Fig. 6 B). Due to the low oxygen content, CO_2RR already becomes the dominant (> 50 % FE) reaction starting from 50 mA/cm^2 and reaches a $FE_{HCOO^-} = 85.80 \pm 4.28$ % at 300 mA/cm^2. A complete breakdown of the FEs for all current densities and oxygen contents can be found in the SI tables 1–4. The introduction of 3 % and 6 % O_2 needs at least an operating current density of respectively 50 and 100 mA/cm^2 to detect any CO_2RR products or respectively 150 and 250 mA/cm^2 for it to become the dominant electrochemical reaction. The required potential to sustain the demanded total current density is also strongly related to the dominant reaction (Fig. 6 D). For example, at 25 mA/cm^2, the 3 % and 6 % O_2 result in a similar potential of -0.86 ± 0.01 V and -0.88 ± 0.05 V because ORR is the only reaction that occurs (no CO_2RR products detected). At the same current density, the potential with a pure CO_2 stream reads -1.67 ± 0.05 V since the CO_2RR to $HCOO^-$ (FE = 95.65 ± 6.98 %) acts as the dominant reaction and typically requires more negative potentials under the given operating conditions and reactor configuration. For a 1% O_2 stream at 25 mA/cm^2, the potential lies inbetween those two potentials (-1.24 ± 0.06 V) due to the interplay between both reactions. This is a consequence of O_2 mass transport limitation that is already present at these low currents and allows some CO_2 to react to $HCOO^-$. Consequently, the required potentials should ultimately converge to the potential response for pure CO_2 with increasing current density, since CO_2RRs consume an ever increasing share of the supplied electrons as the ORR becomes increasingly mass transfer limited. This behavior is indeed observed (see Fig. 6 D) since the potential at 300 mA/cm^2 of O_2-containing streams converges to that without O_2 in the feed.

The results with a Ag-coated GDE are presented in a similar manner by Fig. 6 E-H. The suppression of the hydrogen evolution is more difficult than with Bi_2O_3, especially at 300 mA/cm^2 where $FE_{H_2} = 11.76 \pm 7.91$ % (Fig. 6 G) which is consistent with previous reports [9]. The FE towards the target product CO at 25 mA/cm^2 is almost completely lost when introducing only 1% O_2 ($FE_{CO} = 5.70 \pm 3.53$ %) compared to pure CO_2 ($FE_{CO} = 91.18 \pm 2.69$ %). The FE rapidly restores with increasing current density up to a maximum of 86.08 ± 4.53 % at 150 mA/cm^2 after which it stays more or less constant. The more concentrated 3 % and 6 % O_2 in CO_2 stream need a current density of 75 and 125 mA/cm^2 to detect any significant formation (> 1 % FE) of CO. The potential (Fig. 6 H) follows the same trends as the Bi_2O_3-coated GDE. Only the gaps between potential values of ORR-dominant operating conditions (i.e., low current densities where O_2 mass transport is not limited) are considerably bigger. For example, operating at 25 mA/cm^2 for the 6 % O_2 stream requires a potential of only -0.53 ± 0.11 V compared to a potential of -1.73 ± 0.00 V with pure CO_2 streams. The lower potential in this ORR dominant regime can be explained via the higher catalytic activity of Ag for ORR [29]. Nevertheless, at high current densities also for Ag the potential converges to the value in absence of oxygen, which means that the CO_2RR becomes dominant and the ORR becomes increasingly mass transfer limited. More detailed information on FE values and gap sizes can be found in the SI Tables 5–8.

In essence, the impact of oxygen in the feed stream appears to be minimal when the feed contains low amounts of oxygen (e.g., 1 % O_2)

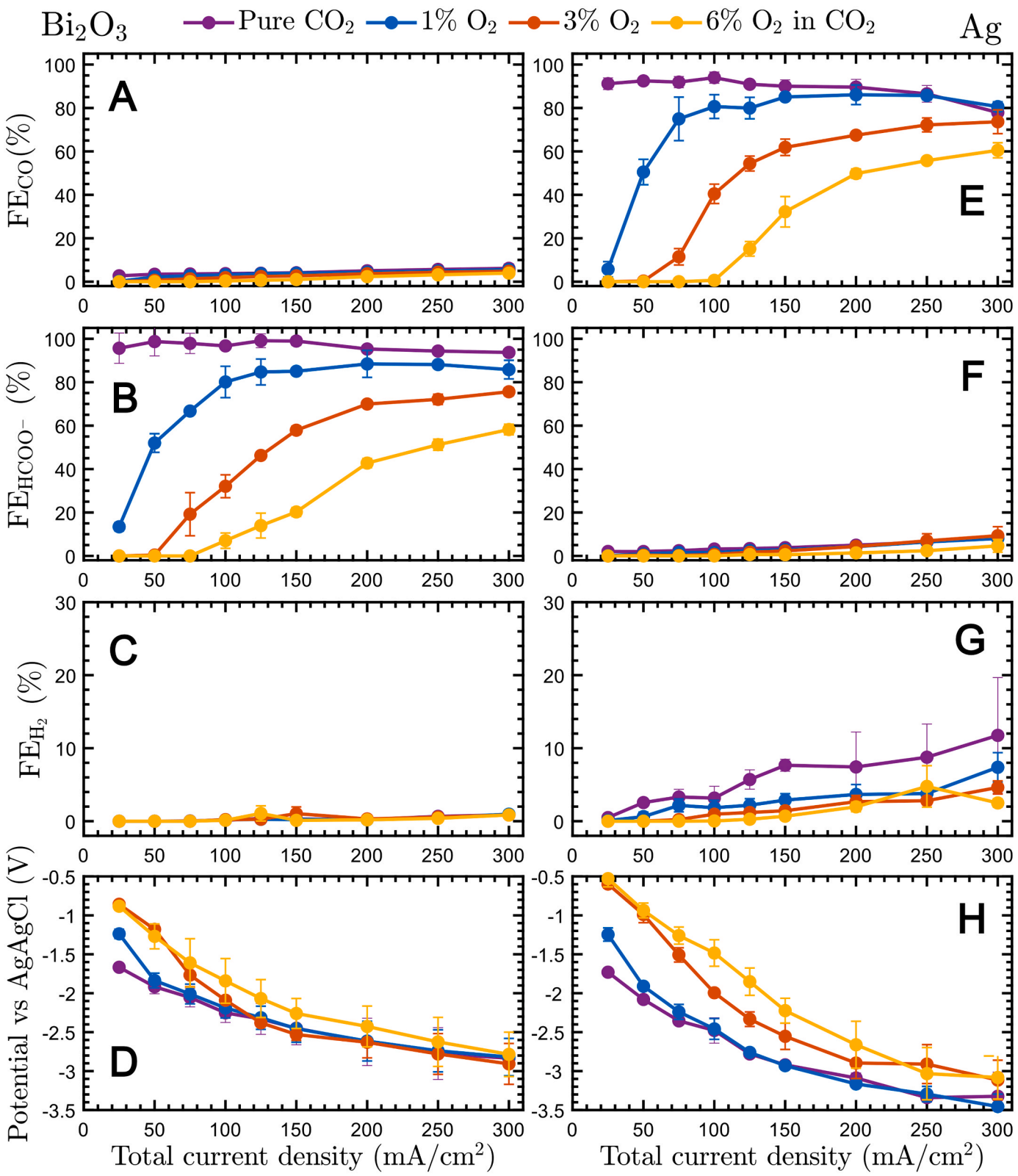

Fig. 6. Faradaic efficiency for CO, $HCOO^-$, H_2 and reference electrode potential for different O_2 concentrations in the CO_2 gas feed stream at 25–300 mA/cm^2 with Bi_2O_3 (A-D) or Ag (E-H) catalyst particles. Error bars represent standard deviation from three experiments.

and an industrially relevant current density is applied (> 100 mA/cm^2) [30,31]. However, as the oxygen content increases, losses in FE become more apparent. Nevertheless, the results shown here indicate that the impact of the ORR can be decreased significantly by supplying high enough current densities as they bring the ORR into the mass transfer limited region and allow the CO_2RR to CO and formate to take over and become the dominant reaction.

3.4. A simple strategy to enhance performance in the presence of oxygen

The results mentioned above suggest that (i) the catalyst stability is not affected by the O_2 impurity and (ii) CO_2RR can take place once there is an O_2 deficiency at the electrode (O_2 mass transport limitation). With this in mind, the question arises whether CO_2RR with O_2-containing feeds can still be more preferable than removing O_2 from the flue gas stream prior to feeding it to the flow reactor. To investigate this further, the current density to C-products and missing current density (due to electron consumption by ORR) is compared (Fig. 7). Especially for a high oxygen content of 6 % O_2 in CO_2, all operating current densities up to 100 mA/cm^2 provide less than 8 mA/cm^2 towards C-products for both Bi_2O_3 (Fig. 7 A) and Ag (Fig. 7 B). From here on, oxygen supply is becoming mass transport limited and CO_2 reduction starts taking over as evidenced by the linear increase of the current density to C-products at further increasing current densities. Note that the ORR rate cannot increase further and consequently, a plateau is observed in Fig. 7 C and D where the missing current density is illustrated. The loss in current density in the region of the plateau for the Bi_2O_3 catalyst is 18.66 ± 3.66 mA/cm^2 (1 % O_2), 58.83 ± 4.65 mA/cm^2 (3 % O_2) and 108.23 ± 7.98 mA/cm^2 (6 % O_2). Similarly, the missing current density with Ag is 16.27 ± 4.77 mA/cm^2 (1 % O_2), 49.37 ± 6.60 mA/cm^2 (3 % O_2) and 97.66 ± 4.43 mA/cm^2 (6 % O_2). From these values, the average current density loss per % O_2 in the feed stream is fixed at 19 ± 3 mA/cm^2/% O_2 or 17 ± 4 mA/cm^2/% O_2 with Bi_2O_3 or Ag respectively. Therefore, the share of electricity cost to reduce O_2 should decrease significantly at high operating current densities. In order to estimate the impact on electricity cost per kg of product output, a voltammetric model from Shin *et al.* [32] was used to calculate the electricity usage for electrolyzer operation at different current densities (SI Figure S.23). Their adapted techno-economic assessment from Jouny *et al.* [33] was then used to illustrate the electricity cost per product output for different oxygen feed concentrations (Fig. 8). At low current densities, all O_2-containing feed streams result in an unfeasible situation where most of the applied current is used for the ORR. This situation changes drastically with increasing operating current density. For example, at 300 mA/cm^2, the extra electricity cost when allowing 3 % O_2 in the feed stream corresponds to only $0.03/kg HCOOH and $0.04/kg CO produced. Knowing

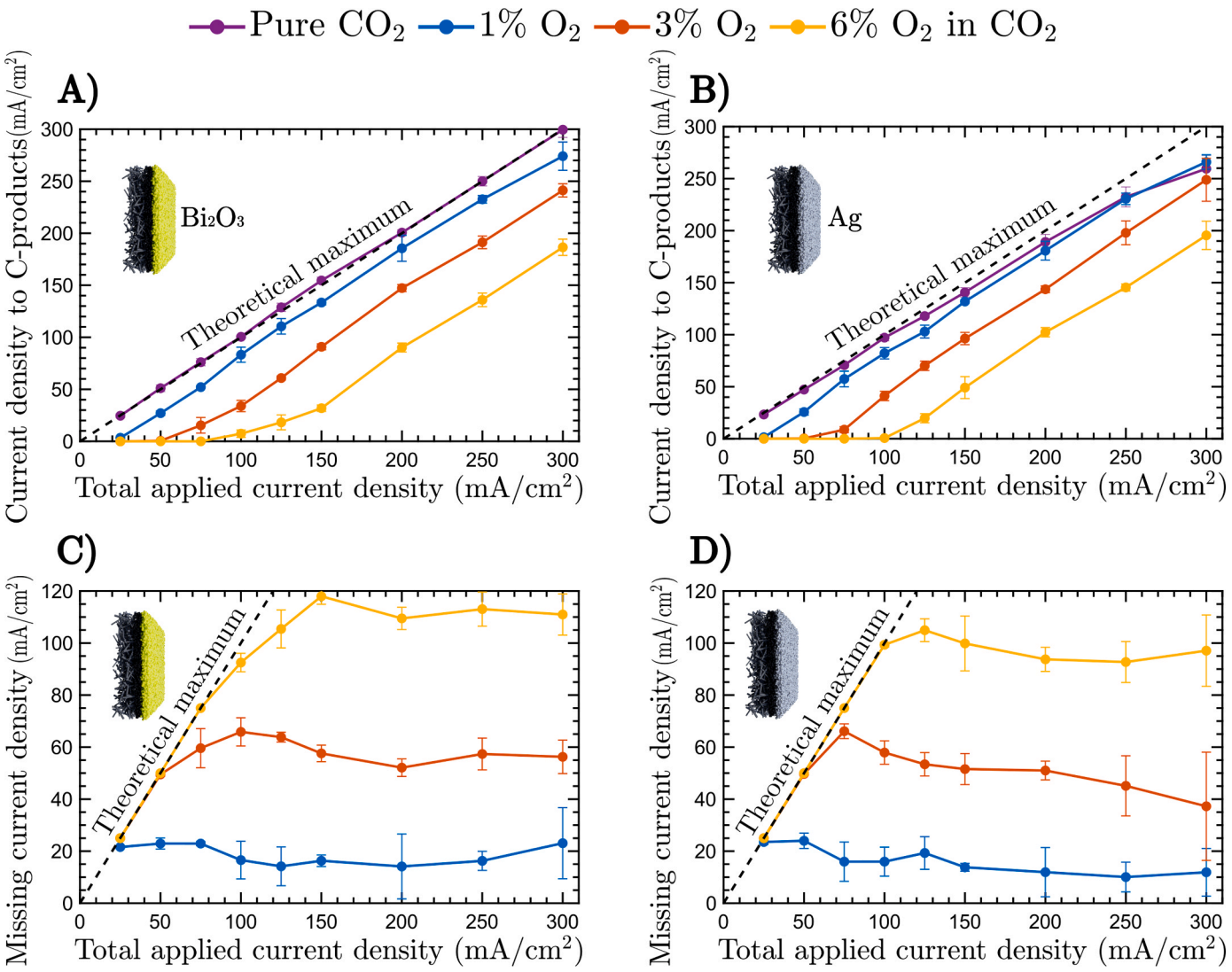

Fig. 7. Current density to carbon products for Bi_2O_3 (A) or Ag catalyst particles (B) and missing current density for Bi_2O_3 (C) or Ag catalyst particles (D). The dashed line indicates the theoretical maximum values that correspond to the total current density that was applied in the experiment.

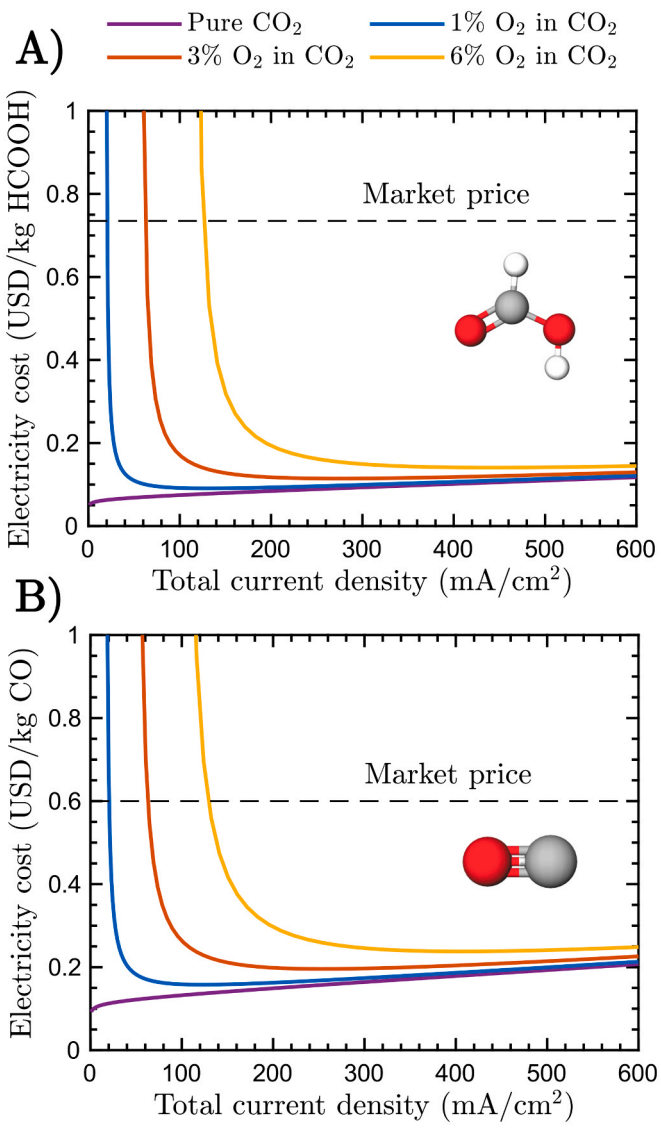

Fig. 8. Required electricity cost per kg of product output for CO_2 electrolyzer operation with target product A) HCOOH and B) CO at different current densities and various feed oxygen concentrations. The dashed line shows the market value per kg product [33].

that the market value of these products are $0.74/kg and $0.6/kg respectively [33], this extra cost accounts only for < 7 % of its market value. Therefore, this analysis indicates that operating the electrolyzer at an increased current density to firstly reduce all O_2 can be a feasible solution. Moreover, an additional benefit of electrochemical systems such as CO_2 electrolyzers comprises the flexibility of the technology. These reactors can easily be shut off and on, simply by applying or removing any current or potential. For example, the reactors can thus be programmed to operate in situations where excess electricity is available and costs are minimal. Finally, some flue gas sources have a moderate to low oxygen content (< 4 % O_2) which makes the complete reduction of O_2 species before CO_2RR in electrolyzers a potential solution [10,11]. In addition to the findings presented here, a further investigation involving highly diluted CO_2 with O_2 as feed stream showed that efficient operation remains challenging under these specific conditions (SI Fig. S.24, S.25). While the previous results significantly raise interest into the pathway of utilizing impure CO_2 feed streams, more hurdles need to be overcome if highly diluted CO_2 streams that contain O_2 would be used a resource for the production of CO and formate.

4. Conclusion

The direct utilization of CO_2 in flue gases omits the need for energy intensive carbon capture steps and is an interesting pathway to explore the economical viability of the technology. Therefore, knowledge about the influence of impurities in CO_2 streams is crucial, as their presence may have a significant impact on the performance of CO_2 electrolyzers. First of all, stability experiments with 198 ppm SO_2 in CO_2 and 213 ppm NO in CO_2 were conducted using Bi_2O_3 and Ag as catalysts. The results demonstrate a stable performance and high Faradaic efficiencies (> 90 %) to the target products over the course of 20 h. Additionally, the influence of oxygen impurities in the feed stream of a CO_2 electrolyzer was studied. The presence of oxygen in flue gas streams at concentrations of several percent is common and cause a decrease in FE to target product CO or $HCOO^-$ during electrolysis due to the oxygen reduction reaction which occurs more preferentially than CO_2RR. Once oxygen supply becomes mass transport limited at the cathode, CO_2RR can take over such that high partial current density to C-products (> 100 mA/cm^2) can be reached by increasing the total operating current density. A potential strategy to reduce the detrimental effects of allowing O_2 in the feed stream is to operate the electrolyzer at a sufficiently high total current density to ensure all O_2 at the electrode is reduced and CO_2RR becomes the dominant reaction. Although this approach takes the penalty of higher electricity usage, the associated costs seem negligible for low O_2-containing feed streams (≤3 % O_2) at 300 mA/cm^2. These results not only offer new insights into the impact of gaseous impurities during CO_2 electrolysis, but also suggest a strategy to improve electrolyzer performance with O_2-containing feed streams.

Additionally, future work could focus on a dedicated techno-economic assessment for the direct utilization of O_2-containing CO_2 feed streams in comparison to the cost of installing and operating purification units to separate O_2 from CO_2. Besides this, investigating the effect of temperature on the CO_2RR with impure CO_2 should be considered in further studies since impurities (especially SO_2) can potentially poison the catalyst at elevated temperatures. Lastly, future work should focus on ways to inhibit the ORR and enhance the Faradaic efficiency to C-products for O_2-containing feed streams. This reduces the extra electricity cost and make the technology more economically viable.

Acknowledgment

This project was funded by the Interreg 2 Seas-Program 2018–2022 in the framework of E2C (Electrons to high value chemical products) and the Flanders Industry Innovation Moonshot program (CAPTIN-2 - HBC.2021.0255). Saskia Hoekx acknowledges financial support from the Research Foundation Flanders (Grant number 1S42623N). The authors want to thank Järi Van den Hoek for his assistance with the XRD measurements.

CRediT authorship contribution statement

Sam Van Daele: Writing – Original Draft, Conceptualization, Investigation. **Lieven Hintjens**: Writing – review & editing, Conceptualization. **Saskia Hoekx**: Writing – review & editing, Investigation. **Barbara Bohlen**: Writing – review & editing, Investigation. **Sander Neukermans**: Writing – review & editing, Conceptualization, Supervision. **Nick Daems**: Writing – review & editing, Supervision. **Jonas Hereijgers**: Writing – review & editing, Supervision. **Tom Breugelmans**: Writing – review & editing, Project administration, Funding acquisition.

Declaration of Competing Interest

The authors declare the following financial interests/personal relationships which may be considered as potential competing interests:

All authors report financial support was provided by the Interreg 2 Seas-Program 2018–2022 in the framework of E2C (Electrons to high value chemical products) and the Flanders Industry Innovation Moonshot program (CAPTIN-2 - HBC.2021.0255). Saskia Hoekx reports financial support was provided by Research Foundation Flanders (Grant number 1S42623N).

Data availability

Data will be made available on request.

Appendix A. Supporting information

Supplementary data associated with this article can be found in the online version at doi:10.1016/j.apcatb.2023.123345.

References

[1] K.M.K. Yu, I. Curcic, J. Gabriel, S.C.E. Tsang, Recent advances in CO_2 capture and utilization, ChemSusChem: Chem. Sustain. Energy Mater. 1 (11) (2008) 893–899.
[2] D. Wakerley, S. Lamaison, J. Wicks, A. Clemens, J. Feaster, D. Corral, S.A. Jaffer, A. Sarkar, M. Fontecave, E.B. Duoss, S. Baker, E.H. Sargent, T.F. Jaramillo, C. Hahn, Gas diffusion electrodes, reactor designs and key metrics of low-temperature CO_2 electrolysers, Nat. Energy 7 (2022) 130–143, https://doi.org/10.1038/s41560-021-00973-9.
[3] C. Chen, J.F.K. Kotyk, S.W. Sheehan, Progress toward commercial application of electrochemical carbon dioxide reduction, Chem 4 (11) (2018) 2571–2586.
[4] M.Y. Lee, K.T. Park, W. Lee, H. Lim, Y. Kwon, S. Kang, Current achievements and the future direction of electrochemical co2 reduction: a short review, Crit. Rev. Environ. Sci. Technol. 50 (2020) 769–815, https://doi.org/10.1080/10643389.2019.1631991.
[5] R.I. Masel, Z. Liu, H. Yang, J.J. Kaczur, D. Carrillo, S. Ren, D. Salvatore, C. P. Berlinguette, An industrial perspective on catalysts for low-temperature CO_2 electrolysis, Nat. Nanotechnol. 16 (2021) 118–128, https://doi.org/10.1038/s41565-020-00823-x.
[6] C. Kolster, E. Mechleri, S. Krevor, N. MacDowell, The role of CO_2 purification and transport networks in carbon capture and storage cost reduction, Int. J. Greenh. Gas. Control 58 (2017) 127–141.
[7] X. Li, J. Liu, W. Jiang, G. Gao, F. Wu, C. Luo, L. Zhang, Low energy-consuming co2 capture by phase change absorbents of amine/alcohol/h2o, Sep. Purif. Technol. 275 (2021), 119181.
[8] T. Al-Attas, S.K. Nabil, A.S. Zeraati, H.S. Shiran, T. Alkayyali, M. Zargartalebi, T. Tran, N.N. Marei, M.A. AlBari, H. Lin, et al., Permselective mof-based gas diffusion electrode for direct conversion of CO_2 from quasi flue gas, ACS Energy Lett. 8 (2022) 107–115.
[9] S.V. Daele, L. Hintjens, J.V. denHoek, S. Neukermans, N. Daems, J. Hereijgers, T. Breugelmans, Influence of the target product on the electrochemical reduction of diluted co2 in a continuous flow cell, J. CO_2 Util. 65 (2022), 102210, https://doi.org/10.1016/j.jcou.2022.102210.
[10] R.P. Singh, K.A. Berchtold, Water treatment and water-vapor recovery using advanced thermally robust membranes for power production, Mater., Phys. Appl. 9 (2019).
[11] X. He, M.-B. Hägg, Energy efficient process for CO_2 capture from flue gas with novel fixed-site-carrier membranes, Energy Procedia 63 (2014) 174–185.
[12] Z. Dai, S. Fabio, N.G. Marino, C. Riccardo, L. Deng, Field test of a pre-pilot scale hollow fiber facilitated transport membrane for CO_2 capture, Int. J. Greenh. Gas. Control 86 (2019) 191–200.
[13] F. Scala, A. Lancia, R. Nigro, G. Volpicelli, Spray-dry desulfurization of flue gas from heavy oil combustion, J. Air Waste Manag. Assoc. 55 (1) (2005) 20–29.
[14] X. Xu, C. Song, B.G. Miller, A.W. Scaroni, Adsorption separation of carbon dioxide from flue gas of natural gas-fired boiler by a novel nanoporous "molecular basket" adsorbent, Fuel Process. Technol. 86 (14–15) (2005) 1457–1472.
[15] M. He, C. Li, H. Zhang, X. Chang, J.G. Chen, W.A. Goddard, M. jeng Cheng, B. Xu, Q. Lu, Oxygen induced promotion of electrochemical reduction of CO_2 via co-electrolysis, Nat. Commun. 11 (2020) 3844, https://doi.org/10.1038/s41467-020-17690-8.
[16] Y. Zhai, L. Chiachiarelli, N. Sridhar, Effect of gaseous impurities on the electrochemical reduction of CO $_2$ on copper electrodes, ECS Trans. 19 (2009) 1–13, https://doi.org/10.1149/1.3220175.
[17] S. Komatsu, M. Tanaka, A. Okumijra, A. Kungi, Preparation of cu-solid polymer electrolyte composite electrodes and application to gas-phase electrochemical reduction of CO_2, Electrochim. Acta 40 (1995) 745–753.
[18] Y. Xu, J.P. Edwards, J. Zhong, C.P. O'Brien, C.M. Gabardo, C. McCallum, J. Li, C. T. Dinh, E.H. Sargent, D. Sinton, Oxygen-tolerant electroproduction of c2 products from simulated flue gas, Energy Environ. Sci. 13 (2020) 554–561, https://doi.org/10.1039/c9ee03077h.
[19] B.H. Ko, B. Hasa, H. Shin, E. Jeng, S. Overa, W. Chen, F. Jiao, The impact of nitrogen oxides on electrochemical carbon dioxide reduction, Nat. Commun. 11 (2020) 5856, https://doi.org/10.1038/s41467-020-19731-8.
[20] W. Luc, B.H. Ko, S. Kattel, S. Li, D. Su, J.G. Chen, F. Jiao, So2-induced selectivity change in CO_2 electroreduction, J. Am. Chem. Soc. (2019) 9902–9909, https://doi.org/10.1021/jacs.9b03215.
[21] M. Duarte, B.D. Mot, J. Hereijgers, T. Breugelmans, Electrochemical reduction of CO_2: Effect of convective CO_2 supply in gas diffusion electrodes, ChemElectroChem 6 (2019) 5596–5602, https://doi.org/10.1002/celc.201901454.
[22] R. Kuwertz, C. Kirstein, T. Turek, U. Kunz, Influence of acid pretreatment on ionic conductivity of nafion membranes, J. Membr. Sci. 500 (2016) 225–235, https://doi.org/10.1016/j.memsci.2015.11.022.
[23] D.C. Bell, A.J. Garratt-Reed, Energy Dispersive X-Ray Analysis in the Electron Microscope, Vol. 49, Garland Science,, 2003.
[24] K.V. Daele, B.D. Mot, M. Pupo, N. Daems, D. Pant, R. Kortlever, T. Breugelmans, Sn-based electrocatalyst stability: a crucial piece to the puzzle for the electrochemical CO_2 reduction toward formic acid, ACS Energy Lett. 6 (2021) 4317–4327, https://doi.org/10.1021/acsenergylett.1c02049.
[25] S. Liu, B. Hu, J. Zhao, W. Jiang, D. Feng, C. Zhang, W. Yao, Enhanced electrocatalytic CO_2 reduction of bismuth nanosheets with introducing surface bismuth subcarbonate, Coatings 12 (2022) 233, https://doi.org/10.3390/coatings12020233.
[26] X. Ge, A. Sumboja, D. Wuu, T. An, B. Li, F.T. Goh, T.A. Hor, Y. Zong, Z. Liu, Oxygen reduction in alkaline media: from mechanisms to recent advances of catalysts, ACS Catal. 5 (8) (2015) 4643–4667.
[27] J.S. Spendelow, A. Wieckowski, Electrocatalysis of oxygen reduction and small alcohol oxidation in alkaline media, Phys. Chem. Chem. Phys. 9 (21) (2007) 2654–2675.
[28] L.C. Weng, A.T. Bell, A.Z. Weber, Modeling gas-diffusion electrodes for CO_2 reduction, Phys. Chem. Chem. Phys. 20 (2018) 16973–16984, https://doi.org/10.1039/c8cp01319e.
[29] R. Sui, X. Zhang, X. Wang, X. Wang, J. Pei, Y. Zhang, X. Liu, W. Chen, W. Zhu, Z. Zhuang, Silver based single atom catalyst with heteroatom coordination environment as high performance oxygen reduction reaction catalyst, Nano Res. 15 (9) (2022) 7968–7975.
[30] S. Verma, Y. Hamasaki, C. Kim, W. Huang, S. Lu, H.R.M. Jhong, A.A. Gewirth, T. Fujigaya, N. Nakashima, P.J. Kenis, Insights into the low overpotential electroreduction of CO_2 to co on a supported gold catalyst in an alkaline flow electrolyzer, ACS Energy Lett. 3 (2018) 193–198, https://doi.org/10.1021/acsenergylett.7b01096.
[31] B. Endrődi, G. Bencsik, F. Darvas, R. Jones, K. Rajeshwar, C. Janáky, Continuous-flow electroreduction of carbon dioxide, Prog. Energy Combust. Sci. 62 (2017) 133–154, https://doi.org/10.1016/j.pecs.2017.05.005.
[32] H. Shin, K.U. Hansen, F. Jiao, Techno-economic assessment of low-temperature carbon dioxide electrolysis, Nat. Sustain. 4 (10) (2021) 911–919.
[33] M. Jouny, W. Luc, F. Jiao, General techno-economic analysis of CO_2 electrolysis systems, Ind. Eng. Chem. Res. 57 (6) (2018) 2165–2177.